

## Electrochemical Characterization and Solid Electrolyte Interface Modeling of $\text{LiNi}_{0.5}\text{Mn}_{1.5}\text{O}_4$ -Graphite Cells

To cite this article: Vittorio Giai Pron *et al* 2019 *J. Electrochem. Soc.* **166** A2255

View the [article online](#) for updates and enhancements.



### **ECS 244<sup>th</sup> Electrochemical Society Meeting**

October 8–12, 2023 • Gothenburg, Sweden

50 symposia in electrochemistry & solid state science

Abstract submission deadline:  
**April 7, 2023**

Read the call for papers &

**submit your abstract!**



# Electrochemical Characterization and Solid Electrolyte Interface Modeling of LiNi<sub>0.5</sub>Mn<sub>1.5</sub>O<sub>4</sub>-Graphite Cells

Vittorio Giai Pron,<sup>1</sup> Daniele Versaci,<sup>1</sup> Julia Amici,<sup>1</sup> Carlotta Francia,<sup>1</sup> Massimo Santarelli,<sup>2</sup> and Silvia Bodourdo <sup>1,2</sup>

<sup>1</sup>Department of Applied Science and Technology, Politecnico di Torino, Turin 10129, Italy

<sup>2</sup>Department of Energy, Politecnico di Torino, Turin 10129, Italy

In this work an electrochemical model combined with an aging model based on SEI formation is developed. Galvanostatic cycling and impedance tests are performed to optimize the cell model by determining parameters for which there is no consensus in literature. The electrochemical model is a P2D model while the aging model is a 0D model. Besides being the first work concerning modeling of LMNO-Graphite cells, relevant aspects of this approach are related to experimental estimation of most parameters involved; a two-steps validation that allows to obtain more significant values of non-experimental parameters (with high accuracy of results); the ability to simulate precisely the spectrum phenomena occurring within the cell and the possibility to consider the Coulombic efficiency of the system.

© 2019 The Electrochemical Society. [DOI: 10.1149/2.0941910jes]

Manuscript submitted February 12, 2019; revised manuscript received May 1, 2019. Published June 27, 2019.

Electrical energy storage technologies play a significant role in the demand for green and sustainable energy. Rechargeable batteries such as Li-ion batteries, Na-ion batteries and Mg-ion batteries, reversibly convert between chemical and electrical energy via redox reactions, thus storing the energy as chemical potential in the electrodes. Among all the energy storage systems, Li-ion technology is widely recognized as the most important for portable electronics, power tools and hybrid/full electric vehicles because of its high power and energy density with respect to others.<sup>1,2</sup> Besides, the high energy density of Li-ion batteries (LIBs) allows their use in electric grid applications, including storage of intermittent and discontinuous energy harvested from wind, solar, geothermal and other renewable sources, thus contributing to widespread use and building an energy-sustainable economy. Therefore, LIBs are of interest for both industry and government funding agencies, thus research in the field has abounded in recent years.<sup>3</sup> However, further improvements to currently available LIBs technology are needed to meet some of the requirements for automotive application, such as an acceptable single-charge driving range, higher efficiency, higher safety and lower costs. In particular, the main limitation preventing the use of LIBs in electric vehicles consists in their low gravimetric and volumetric energy densities compared to traditional fuels.

Modeling of LIBs has kept pace with development of different battery chemistries. The first commercial Lithium-ion battery was developed in 1991 by Sony and the first physical model, a pseudo 2D model, similar to that used in this work, was already developed in 1992<sup>4</sup> borrowing from modeling approaches from non-Lithium based batteries. During the years, other approaches were developed, based on phase field modeling or multiscale modeling.<sup>5-7</sup> The current objectives of modeling remain the same, i.e. improve understanding, support design and optimization and scaling up battery systems. In addition, physical models are expected to be used online on future BMS, due to their superior accuracy and predictive capabilities compared to black box models.<sup>8</sup> Though LIBs modeling has undergone big changes in terms of complexity and inclusion of different phenomena, the basic approach and electrochemistry still borrows from the first models by Newman et al.<sup>9,4,10,11</sup>

Considering that the most commercialized anode material is Graphite (for its non-toxicity, low-cost, high theoretical capacity and low open circuit potential), the cathode material plays the main role in determining performance and costs of LIBs.<sup>12</sup> Unfortunately, most of current cathode materials, e.g. LiNi<sub>0.8</sub>Co<sub>0.15</sub>Al<sub>0.05</sub>O<sub>2</sub> (NCA), LiNi<sub>1/3</sub>Co<sub>1/3</sub>Mn<sub>1/3</sub>O<sub>2</sub> (NMC), LiMn<sub>2</sub>O<sub>4</sub> (LMO) and LiFePO<sub>4</sub> (LFP), are either costly, toxic or unable to ensure sufficient energy density. Consequently, major research efforts are focused on improving the positive electrode active material.

The energy density of rechargeable batteries is determined by multiplying the specific capacity of electrodes for the working cell voltage<sup>3</sup>; therefore, LIBs energy density can be increased either by increasing specific capacity and/or operative voltage.<sup>13,14</sup> One possible solution to raise the operating potential is the use of so-called high potential cathodes (about 5 V). In such frame, Lithium Nickel Manganese oxide spinel (LiNi<sub>0.5</sub>Mn<sub>1.5</sub>O<sub>4</sub>, LNMO) is one of the most promising candidates to be combined with graphite anodes, because of its high theoretical specific capacity (147 mA h g<sup>-1</sup>), high nominal operating voltage (4.7 V vs Li<sup>+</sup>/Li), high thermal stability and low cost.<sup>12,15,16</sup> Intensive research efforts have been directed to unravel the influence of morphology and transition-metal order on the electrochemical performances.<sup>14,17-20</sup> However, in case of cells with high potential cathodes and Graphite anodes, important factors are formation of Solid Electrolyte Interface (SEI) during initial stages of aging and electrolyte degradation. SEI prevents solvent co-intercalation and Graphite exfoliation but it is also responsible for active Lithium consumption and solvent reduction reactions, resulting in irreversible capacity losses. This is described by Equation 1, in which  $S$  is the electrolyte solvent and  $P_{SEI}$  depicts the products of degradation reactions, (e.g. LiF, Li<sub>2</sub>CO<sub>3</sub>, LiF and Li<sub>2</sub>O):



The aim of this work is twofold. First, we further investigated SEI formation mechanisms in high-potential LIBs through the study of its dependence on charge/discharge currents. Second, we developed a complete cell model, which is valid over the entire range of operational currents. These achievements were obtained coupling the widely used pseudo-2D (P2D) electrochemical model with the 0D capacity fade model to study for the first time the SEI behavior of LMNO-Graphite full cell. To this purpose, each cell material was fully characterized and an experimental analysis of the influence of the charge/discharge current on the capacity fade in the first twenty cycles of the cells was performed. Finally, the electrochemical and capacity fade models were implemented (through the software COMSOL Multiphysics) and experimentally validated.

## Experimental

Since new materials are used, their properties are not yet available in literature. Thus, it was necessary to characterize them from an electrochemical point of view in order to obtain the required inputs of the models and key parameters allowing the comparison of these novel materials with the ones commonly used in Lithium-ion batteries.

**Electrode preparation.**—As far as the electrode composition is concerned, the cathode consisted of 90 wt% of active material LNMO (LiNi<sub>0.5</sub>Mn<sub>1.5</sub>O<sub>4</sub>, NANOMYTE-SP10, NEI corp.), 5 wt% of

<sup>a</sup>E-mail: silvia.bodourdo@polito.it

conducting Carbon Black (C65 Imerys Carb.) and 5 wt% of binder PVDF (Kynar, Arkema). The anode consisted of 96.5 wt% of Graphite (SLS30 Imerys Carb.), 0.5 wt% of Carbon Black (C45 Imerys Carb.) and 3 wt% of binders CMC (2%<sub>in</sub>, Daicel 2200) and SBR (1%<sub>in</sub>, JSR TRD102A). The electrolyte was provided by Arkema, it was a 1.0 M solution of LiPF<sub>6</sub> in EC:EMC 3<sub>v</sub>:7<sub>v</sub> and additives in order to increase cell stability at high potentials avoiding electrolyte degradation, (additives amount and type are under patent by Arkema/Cea). For each electrode, disks of 0.8 cm<sup>2</sup> (T-cell assembly) and 2 cm<sup>2</sup> (coin-cell assembly) were punched out, vacuum dried at 150°C (Büchi Glass Oven B-285) for 4 h. Electrodes were weighted and assembled inside an Argon-filled dry glove-box (MBraun Labstar; H<sub>2</sub>O and O<sub>2</sub> content lower than 1 ppm). For the electrochemical characterization, 2032 Coin cell and Polypropylene three-electrode T-cells were used, using lithium foil (Chemetall Foote Corporation) both as counter and reference electrodes in half-cell configuration. Two glass-fiber disks (Whatmann GF/A) with 0.1 mm thickness each were used as separators. To validate the aging models only the data obtained with coin cell assembly were considered because of the higher stability showed with such cell design.

**Morphological analysis.**—Morphological analysis was focused on determining the order of magnitude of particle size in active materials. Morphological analysis of samples was performed by FESEM (Field Emission Scanning Electron Microscopy) using a Zeiss SUPRA 40 with Gemini column and Schottky field emission source (Tungsten at 1800 K). Acquisitions were carried out by setting an acceleration potential (EHT) of 5 kV, working distance (WD) between 2.3÷3.1 mm and magnification of 40 kX (scales of 100 nm).

**Electrical conductivity.**—For the electrical conductivity of electrode materials, the four-point method was opted as standard methodology to measure indirectly the resistivity of the material. The method is particularly suitable when small samples are available (size of the order of mm). It can be used when the distance between the probes is small with respect to the smallest dimension (excluding the thickness) of the sample and when no probe is excessively close to the edge of the sample itself. A detailed description of the method was proposed by Valdes et al.<sup>21</sup> providing, for different geometries a functional relationship between the electrical resistivity of the material,  $\rho_e$ , and the ratio between the measured voltage and the applied current. The set up consisted of the four points probe positioned onto the surface material. An electrostatic potential was applied in the inner contacts meanwhile the electrical current ( $I$ ) was measured between the outer contacts. The curve  $I$  vs. V was obtained by VMP3 potentiostat. A linear function  $I$  vs. V was plotted, which slope corresponds to the inverse of resistance.

**Electrochemical impedance spectroscopy.**—Electrochemical impedance spectroscopy measurements (EIS) were carried out by CH I660d Electrochemical Workstation in potentiostatic mode (PEIS) using 10 mV voltage amplitude. The resulting Nyquist and Bode spectra were subsequently modeled using equivalent circuit and electrochemical models. EIS were performed on pristine cells in order to obtain significant results for the parametrization of electrode and electrolyte materials.

**Galvanostatic cycling.**—The galvanostatic cycling tests were performed by BR-200 multi-channel Arbin Instrument. All tests were carried out in the potential window of 2.5 - 4.9 V. Measurements were carried out on several cells with same materials in order to ensure reproducible results.

## Modeling

**Electrochemical model.**—The simulation model of the cells electrochemical behavior is based on a pseudo-two dimensional (P2D) approach, in which one dimension is the thickness of the cell and the other is the spherical particle dimension. P2D model represents a good

approximation of the battery while keeping the model computationally inexpensive as the significant direction of variation in properties is along the thickness of the cell. Current flow can be assumed to be uniform and perpendicular to the current collector sheets for practical purposes if conductivities of the sheets are higher compared to the electrodes.<sup>4,8,11,22,23</sup> Given the electrode morphology, and in order to keep the model simple, the model taken in consideration is the so-called “porous-electrode model”. This means that our electrode being highly porous and being the pores filled with highly conductive liquid electrolyte, the only reaction considered is the insertion reaction of Lithium ions on the surface of electrode active materials. Indeed, this phenomenon is supposed to be kinetically predominant, making others such as solid diffusion almost negligible. This is described by Equation 2 in which  $\theta_s$  and  $Li\theta_s$  represent either free or occupied reaction site on the surface of the active material, respectively.



Therefore, considering as constant the total concentration  $c_{s,max}$  of the reaction sites within each electrode, the free sites concentration of the active material  $c_{fs}$  on the surface is directly provided by Equation 3 in which  $c_s$  represents the volumetric concentration of Lithium inside the electrodes.

$$c_{fs} = c_{s,max} - c_s \quad [3]$$

The maximum concentration of Lithium-ions inside the electrodes can be evaluated by considering that at least one Lithium atom for each molecule of active material can be stored in both LiNi<sub>0.5</sub>Mn<sub>1.5</sub>O and LiC<sub>6</sub>. Therefore, for each electrode the maximum concentration of Lithium-ions within the active material can be expressed through Equation 4 in which  $PM_{mat,el}$  and  $\rho_{mat,el}$  are the molecular weight and the density of the active material inside the electrode, respectively. The molecular weight of the active material can be calculated from the molecular weight of the constituent elements.

$$c_{s,max} = \frac{1}{\rho_{mat,el} PM_{mat,el}} \left[ \frac{mol/L}{mol/m^3} \right] \quad [4]$$

For each electrode, the maximum theoretical gravimetric energy density of the active material  $Q_{h,el}$  can be expressed through the Faraday Law (Equation 5) in which  $z$  is the number of electrons transferred per ions,  $F$  is the Faraday constant and  $M_{mat,el}$  is the mass of active material in the electrode.

$$\frac{Q_{h,el}}{M_{mat,el}} = \frac{PM_{mat,el}}{zF} \quad [5]$$

An important parameter for insertion of Lithium into active materials is the State-of-Charge ( $SoC$ ), which can be defined as the ratio between the volumetric concentration of Lithium inside the electrode  $c_s$  and the maximum Lithium concentration that can be stored within it  $c_{s,max}$  (Equation 6). Since the volumetric Lithium concentration inside each electrode is composed of a binary electrolyte and a single-phase polymeric solvent. Hence, to model the corresponding region, the theory of concentrated solutions was used to comply with the concentration levels in the battery. Therefore, in the electrolyte-separator domain the model solves the current conservation equation (Equation 7) and the saline mass conservation equation (Equation 8), in which  $c$ / represents the electrolyte conductivity,  $t_+$  is the transference number (around 0.363 in case of LIBs),  $\varepsilon$  is the volumetric concentration of Lithium ions in the electrolyte,  $D_1$  is the salt diffusivity in the electrolyte and

$$SoC = \frac{c_s}{c_{s,max}} = \frac{Q}{Q_h} \quad [6]$$

Along cell thickness, the electrochemical system has been modeled through a single domain consisting of five sub-domains representing two current collectors, two electrodes and the separator. The electrolyte is composed of a binary electrolyte and a single-phase polymeric solvent. Hence, to model the corresponding region, the theory of concentrated solutions was used to comply with the concentration levels in the battery. Therefore, in the electrolyte-separator domain the model solves the current conservation equation (Equation 7) and the saline mass conservation equation (Equation 8), in which  $c$ / represents the electrolyte conductivity,  $t_+$  is the transference number (around 0.363 in case of LIBs),  $\varepsilon$  is the volumetric concentration of Lithium ions in the electrolyte,  $D_1$  is the salt diffusivity in the electrolyte and

$i_t$  is the ionic current flowing into the electrolyte. All the electrolyte transport properties are taken from Ref. 24 in which all parameters are expressed as function of temperature and salt concentration in the electrolyte.

$$\frac{\partial c_t}{\partial t} = \nabla \cdot (D_t \nabla c_t) - \nabla \cdot \left( \frac{i_{it+}}{F} \right) + \frac{\nabla \cdot i_t}{F} \quad [7]$$

The two current collectors are modeled as two simple non-reacting electrodes in which the sole occurring phenomenon is the electronic conduction, described by Ohm law (Equation 9);  $\sigma_s$  represents the electrical conductivity of the current collector and  $i_s$  is the local current density that flows inside.

$$i_s = -\sigma_s \nabla \phi_s \quad [9]$$

The electrodes were modeled through the porous electrode theory, valid for electrodes composed of porous solid phase, which properties are indicated with subscript “ $s$ ”. A liquid phase, which properties are indicated with subscript “ $v$ ”, is contained in the pores of the solid phase and all reactions occur at the interface between the two phases. Therefore, within their related domains the model solves the current conservation both in solid (Equation 10) and in liquid (Equation 11) phases. In the equations,  $i_s$  represents the current density that flows in the electrodes,  $\sigma_s$  is the electric conductivity of the electrode,  $i_{loc}$  is the current density related to the reactions occurring within the electrode and  $i_{NF}$  is the total non-Faradic current density generated in the electrode (e.g. due to existing double layer at the electrode-electrolyte interface).

$$\nabla \cdot i_s = i_{loc} - i_{NF} \quad [10]$$

$$\nabla \cdot i_t = -\nabla \cdot i_s = i_{loc} + i_{NF} \quad [11]$$

Along the radial dimension of the active material particles, the model only solves the Fick law for the diffusion of Lithium ions in the active material (Equation 12) using boundary conditions described by Equation 13.

$$\frac{\partial c_s}{\partial r} = \nabla \cdot (-D_s \nabla c_s) \quad [12]$$

$$\frac{\partial c_s}{\partial r} = 0|_{r=0} - D_s \frac{\partial c_s}{\partial r} = -\frac{\nabla \cdot i_s}{a_v F}|_{r=r_p} \quad [13]$$

In order to account for the reduced volumetric fraction of conductive material in the electrode for the presence of the electrolyte and the greater transport distance due to the tortuosity of the pores, it is possible to use the corrected values of diffusivity and electrical conductivity for porous electrodes materials. These values, which are named “effective”, depend on the structure of the porous materials as well as the phases involved. In the case of LIBs, the effective diffusion coefficient  $D_{eff}$ , the effective conductivity of the liquid phase  $\sigma_{l,eff}$ , and the effective conductivity of the solid phase  $\sigma_{s,eff}$  can be obtained through Equation 14 in which  $\varepsilon_p$  and  $\tau_L$  represent the porosity and the tortuosity of the material, respectively.

$$D_{eff} = \frac{\varepsilon_p}{\tau_L} D_L, \quad \sigma_{l,eff} = \frac{\varepsilon_p}{\tau_L} \sigma_l, \quad \sigma_{s,eff} = \frac{\varepsilon_p}{\tau_L} \sigma_s \quad [14]$$

Here, Bruggeman relationship is considered, according to which tortuosity is a function of material porosity and defined by Equation 15. Therefore, it is possible to rewrite the effective properties of materials through the corresponding effective values  $D_{l,eff}$ ,  $\sigma_{l,eff}$  and  $\sigma_{s,eff}$ .

$$\begin{cases} D_{l,eff} = \varepsilon_p^{1.5} D_l \\ \sigma_{l,eff} = \varepsilon_p^{1.5} \sigma_l \\ \sigma_{s,eff} = \varepsilon_p^{1.5} \sigma_s \end{cases} \quad [15]$$

For each electrode, Equation 16 is used to model the Lithium ions insertion reaction into the electrodes active material. Here,  $i_{tot}$  represents the total current density transferred within the electrode due to  $NR$  reactions taking place within it.  $a_{vi}$  and  $i_{loc,i}$  represent the specific surface (per unit volume) of the particles in the active material and the current density generated by the generic  $i^h$  reaction in the electrode, respectively.

$$i_{tot} = -\sigma_v \nabla \phi_t + \frac{2\sigma_v R T}{F} \left( 1 + \frac{\partial \ln f}{\partial \ln c_t} \right) (1 + t_+) \nabla \ln c_t \quad [8]$$

The chemical kinetics of the Lithium-ion intercalation reaction within the active materials of the electrodes is described by the Butler-Volmer equation (Equation 17), which represents the standard description of the reaction kinetics in electrodes. The theory is almost always applicable because  $i_0$  represents an empirical parameter.

$$i_{loc} = i_0 \left[ \exp \left( \frac{\alpha_a F}{RT} \eta \right) - \exp \left( \frac{\alpha_c F}{RT} \eta \right) \right] \quad [17]$$

The exchange current density used for the model is expressed through Equation 18 in which  $c_{l,ref}$  is a reference concentration for the electrolyte (assumed to be equal to 1 mol m<sup>-3</sup>),  $\alpha_a$  and  $\alpha_c$  are the anodic and cathodic dimensionless transfer coefficients,  $k_a$  and  $k_c$ , expressed in m/s, are the anodic and cathodic rate constants that depend on the materials used in the electrodes and  $c_l$  is the Lithium ions concentration within the electrolyte.

$$i_0 = F (k_c^{\alpha_a}) (k_a^{\alpha_c}) (c_{s,max} - c_s)^{\alpha_a} (c_s)^{\alpha_c} \left( \frac{c_l}{c_{l,ref}} \right)^{\alpha_a} \quad [18]$$

The over-potential due to the electrochemical reactions can be expressed by Equation 19 in which  $\varphi_l$  represents the electrolyte electrical potential and  $OCV$  represents the cell open circuit potential.

$$\eta = \phi_s - \phi_l - OCV \quad [19]$$

The electrochemical model considers also that, in some cases, a capacitive current can flow because of the presence of the double layer at the electrode-electrolyte interface. The double layer can be considered as a parallel plate capacitor since the absolute amount of charge that separates varies with charge density on the electrode and with potential. A widely used empirical method takes into account the influence of the double layer ability to introduce on the polarization curve a constant ideal capacity at the solid electrode-electrolyte interface. The capacitor then stores a charge defined by Equation 20 and contributes to the cell charge with a non-Faradic current density given by the Equation 21, that determines an increase of the measured total current density. In this case, the surface of the double layer is assumed to be equal to the surface of the electrode-electrolyte interface  $a_v$ . Besides, the presence of the capacity of the double layer allows to model the impedance spectrum.

$$Q_{dl} = C_{dl} (\phi_s - \phi_l) \quad [20]$$

$$\dot{I}_{NF} = \frac{dQ}{dt} = \frac{d}{dt} [C_{dl} (\phi_s - \phi_l)] \quad [21]$$

The boundary conditions used in the electrochemical model are listed below:

- the boundary condition “ground”, corresponding to Equation 22, is applied to define a reference potential within the model. In the analyzed cases, this boundary condition is always imposed at the negative electrode of the cell in order to define the cell voltage according to Equation 23.

$$\begin{cases} E_{cell} = \phi_{s,electrode} - \phi_{s,anode} \\ \text{the boundary condition “current density in the electrode”, corresponding to Equation 24, is applied at the extreme of the positive } \\ \text{Bruggeman relationship} \end{cases} \quad [23]$$

$$\phi_{s,anode} = 0 \quad [22]$$

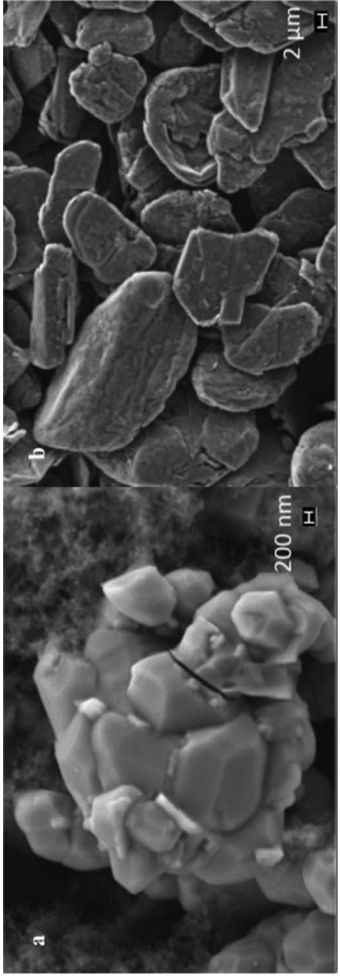


**Figure 1.** FESEM micrographs at different magnifications for electrodes active materials (a) Cathodic active material with a magnification of 40 kX (b) Anodic active material with a magnification of 5 kX.

current collector to model the galvanostatic cycling of the cell. In particular, the value of the current density has to be positive during the cell charge and negative during the cell discharge.

$$-n \cdot i_s = i_{bad,cathode} \quad [24]$$

• the boundary condition “electrode potential”, corresponding to Equation 25, is applied to the extremity of the positive electrode current collector to simulate the constant potential charge/discharge processes and the impedance or voltammetry test. Here, this boundary condition is applied for the simulation of an electrochemical impedance test in which a harmonic perturbation characterized by an amplitude  $V_a$  and a frequency  $f$  is applied to the positive electrode.

$$\phi_{s,cathode} = \phi_{s,bad} = OCV(SoC) + V_a \sin(2\pi f t) \quad [25]$$

**Aging model.**—There are several models in the literature that implement the aging phenomena within LIBs.<sup>25</sup> The simulations for LIBs lifespan estimation are usually based on physical models that typically contain expressions based on empirical expressions. The physical model used in this work allows to predict cell aging by a minimum number of additional parameters with respect to the proposed electrochemical model. Besides, it could be possible to combine the cell degradation model directly in more sophisticated electrochemical models to study the spatial distribution of the degradation effects inside the porous electrodes. Previous models have shown a capacity reduction proportional to  $\rho^{0.5}$  because of the limitation of the diffusion process of the reacting species through the SEI layer.<sup>26,27</sup> The proposed model takes into account the effect of SoC on cell aging (which has been experimentally highlighted), the capacity reduction of the cell, the increase of the potential drop through the negative electrode due to the low SEI electrical conductivity, and the effect of the reduction of the volumetric fraction of electrolyte in the negative electrode on the charge transport in electrolyte.<sup>28,29</sup> The capacity fade of cells is considered as due to SEI formation only. Therefore, the irreversible parasitic reaction in the negative electrode described by Equation 1 is added to the intercalation/de-intercalation reaction of Lithium-ions in the active material of the electrodes. The chemical reaction leading to SEI formation is described by Equation 26 in which  $HK$  represents the dimensionless Graphite expansion coefficient,  $i_{loc,IC,ref}$  the exchange current density related to a 1C charge,  $\eta_{SEI}$  and  $q_{SEI}$  the over-voltage and the loss of capacity due to SEI formation, respectively. The remaining parameters in the equation are called “aging parameters” and were used for the calibration of the aging model.

$$i_{loc,SEI} = -\frac{(1+HK)i_{loc,IC,ref}}{\exp\left(\frac{qF}{RT}\eta_{SEI}\right) + \frac{fI}{i_{loc,IC,ref}}q_{SEI}} \quad [26]$$

In order to account for the SEI layer growth, it was necessary to introduce the independent variable  $c_{SEI}$ , which variation over time is described by Equation 27 representing the volumetric concentration in the negative electrode of the degradation reaction products. Obviously, an increase of  $c_{SEI}$  leads to a decrease of active material volumetric

fraction and of cell capacity. There is a proportional relationship between the concentration  $c_{SEI}$  and the capacity losses due to SEI (Equation 28). The model also takes into account the ohmic over-voltage due to the low electronic conductivity of the SEI layer through the Equation 29.

$$\frac{\partial c_{SEI}}{\partial t} = -\frac{\nu_{SEI}i_{loc,SEI}}{nF} \quad [27]$$

$$q_{SEI} = \frac{F}{A_v}c_{SEI} \quad [28]$$

$$s_{SEI} = c_{SEI} \frac{PM_{SEI}}{a_v \rho_{SEI}} \rightarrow R_{SEI} = \frac{s_{SEI}}{\sigma_{SEI}} \quad [29]$$

## Results and Discussion

**Experimental results.—Morphological analysis.**—Fig. 1 shows FESEM micrographs acquired for cathodic and anodic material, respectively. In the cathode, the active material particles size is slightly reduced compared to the one of the pristine powder reported in the material datasheet (5–7 μm). This can be explained by the material processing during the positive electrode preparation. Therefore, in the electrochemical model an average particle diameter of 4.5 μm was used. For the anode active material, the analysis allowed the evaluation of an equivalent diameter of the planar particles of about 9.93 μm, which is compatible with the dimensions reported on the material powder datasheet ( $D_{10}$ : 8.0 μm).

**Electrical conductivity.**—The functions providing the relationship between the probe resistivity,  $\rho_{el}$ , and the ratio between the measured potential  $V_D$  and the applied current  $I$  for various geometries were evaluated by Uhlir.<sup>31</sup> Such treatment was justified for structures that are three-dimensional and infinite in at least one direction.<sup>32</sup> When the four-point method is applied to a very thin sheet of material, as in this case, the two outermost points of the sample represent a dipole. Having measured the distances between the various probes,  $s_1$ ,  $s_2$  and  $s_3$ , it was possible to calculate the electrical resistivity of the sample through Equation 30. The test was performed several times at different “scan-rates” (i.e. current variation speed) always obtaining the same results that are shown in Fig. 2 where it is possible to observe the measured voltage  $V_D$  as a function of the input current  $I$ . The electrical conductivity obtained for the negative and the positive electrodes are equal to 0.202 S m<sup>-1</sup> and 0.0253 S m<sup>-1</sup>, respectively.

$$\rho_{el} = \frac{V_D}{I} 2\pi \left( \frac{1}{s_1} - \frac{1}{s_1 + s_2} - \frac{1}{s_2 + s_3} + \frac{1}{s_3} \right)^{-1} \quad [30]$$

**Electrochemical impedance spectroscopy.**—The parameters adopted for the EIS measurement are shown in Table 1. Firstly, impedance analysis was performed by assembling two glass fiber

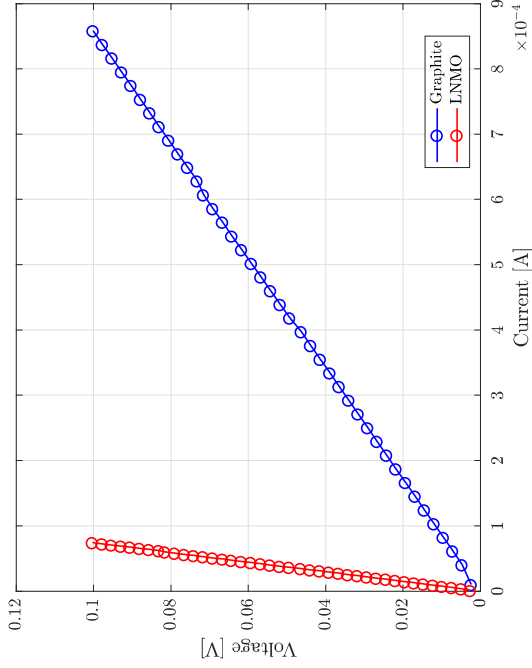


Figure 2. Results of four-probe analysis for the two electrodes.

separators between two stainless steel current collectors in T-cell design in order to calculate the electrolyte electrical conductivity and verify the possibility of using the data reported in the literature.

Obviously, the result is not influenced by the presence of the steel supports as the electrical conductivity is orders of magnitude greater than that of electrolyte. The result obtained at 25°C is shown in Fig. 3 in which the intersection between the real axis and the curve, which abscissa corresponds to the ohmic resistance due to the electrolyte  $R_{el}$ , has been highlighted through a red point. Thus, the behavior of the electrochemical system is purely resistive. The obtained value of the resistance is approximately equal to 2.996 Ohm. Starting from this value, the conductivity of the electrolyte was calculated by using Equation 31 in which  $L_{sep}$  represents the total thickness of the two separators and  $S_{sep}$  is the cell surface. The calculated electrolyte conductivity is equal to 0.899 S/m and perfectly agrees with the value reported in Ref. 24, from which the characteristics of the electrolyte have been taken for the model. Besides, as reported in the Electrochemical model calibration section, a series of impedance tests were carried out on the Lithium-LNMO cathode in half-cell and used in the first phase of calibration of the electrochemical model.

$$\sigma_{el} = \frac{1}{R_{el}} \frac{L_{sep}}{S_{sep}} \quad [31]$$

**Galvanostatic cycling.**—The most important input for the electrochemical model is certainly the trend of the equilibrium potential (Open Circuit Voltage, OCV) as a function of the State of Charge (SoC) and of the temperature of the electrode. The dependence of OCV on SoC was obtained experimentally for all the 120 different charge states. At each step, the electrochemical cell system was relaxed for 3 hours to achieve the equilibrium conditions; thus, the equilibrium potential was calculated as the average value of the cell potential in

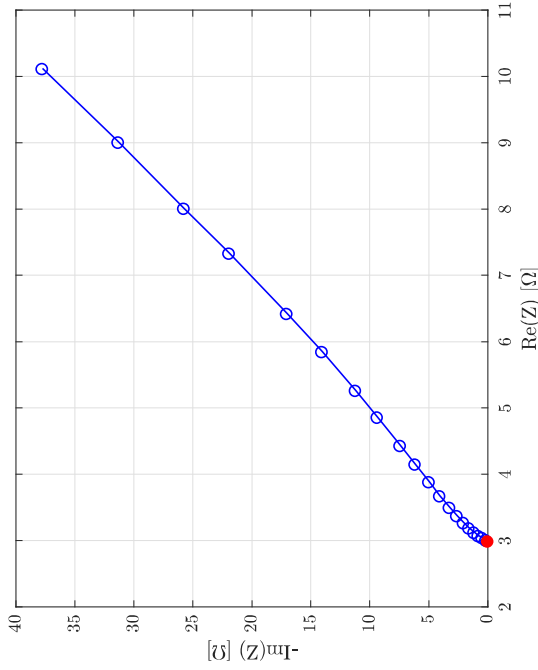


Figure 3. Result of the electrolyte electrical resistivity measurement.

the last two minutes of measurements. The trends of the equilibrium potential as a function of the SoC for the two electrodes are shown in Fig. 4. The results obtained for the negative electrode are perfectly compatible with those reported in literature.<sup>33-36</sup> Thus, as previously mentioned, in order to evaluate the effect of the charge/discharge current on aging of the electrochemical system, several galvanostatic cycling tests were carried out at different C-rates. For each current, 20 charge/discharge cycles were performed to observe aging of cells due to SEI formation, which mainly occurs during the first charge cycles.

**Models calibration and validation.**—*Electrochemical model calibration.*—The electrochemical model calibration was performed in order to determine some of the cathode input parameters, which were not reported in literature. This was not performed for the anode, as the intercalation mechanism in Graphite electrodes is well established.<sup>37,38</sup>

The calibration of positive electrode parameters (e.g., the double layer capacitance, the ionic diffusivity and the rate of the intercalation

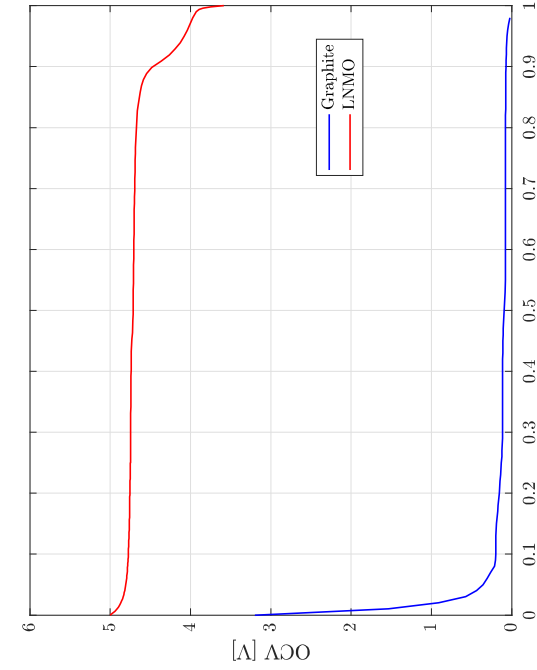
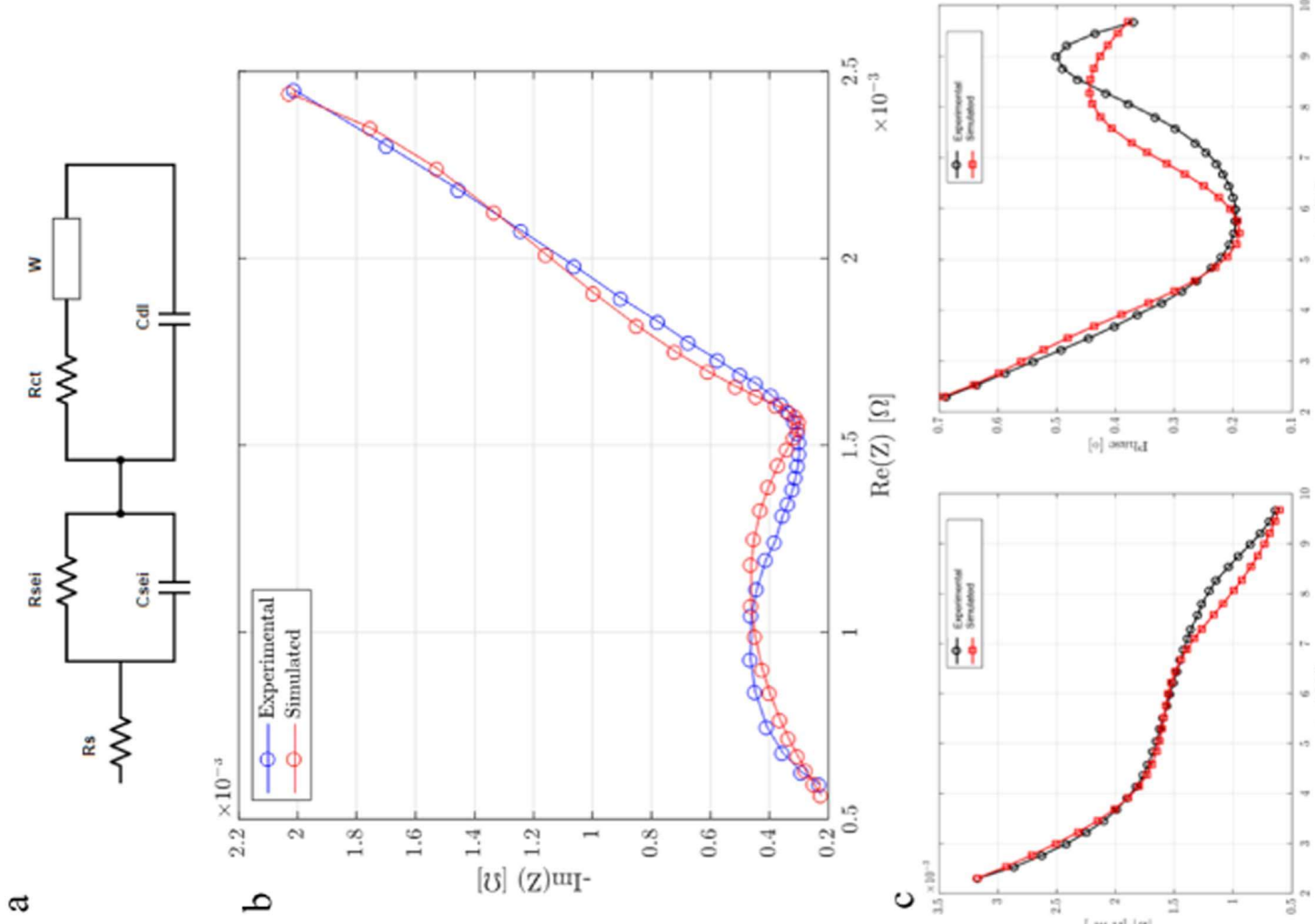


Figure 4. Trend of the equilibrium potential of the two electrodes as a function to their state of charge SoC.

Table I. Tables of parameters for impedance experiments.

Parameter	Value
Frequency range	100 kHz ± 10 mHz
Peak voltage	10 mV
Reference voltage	0 with respect to OCV
Number of points per decade	12



**Figure 5.** Equivalent circuit used for EIS fitting (a), comparison between the experimental and the simulated Nyquist diagrams (b) and comparison between the experimental and simulated Boe diagram (c) resulting from the electrochemical impedance spectroscopy.

reaction in the positive electrode) was carried out through the simulation of the electrochemical impedance spectroscopy on the positive electrode. The first step for calibration was the fitting of simulated EIS spectra to experimental EIS spectra at high frequencies, where the cell is strictly resistive and where the most affecting parameter is the electrical conductivity of the positive electrode (the conductivity of the electrolyte being known). The second step was the determination of the rate of the Lithium intercalation reaction in the positive

electrode active material  $i_0$  through the minima in EIS spectra, where the cell assumes a strictly resistive behavior dependent on  $i_0$ . The third step provided the double layer capacitance at the electrode-electrolyte interface through maxima of the semicircle in the EIS spectra. All the electrolyte properties were taken from Ref. 24. Using the mean radius of the positive electrode particles determined by FESEM and the electrical conductivity of electrodes by four points probe measurements, it was possible to obtain an exchange current density for the Lithium

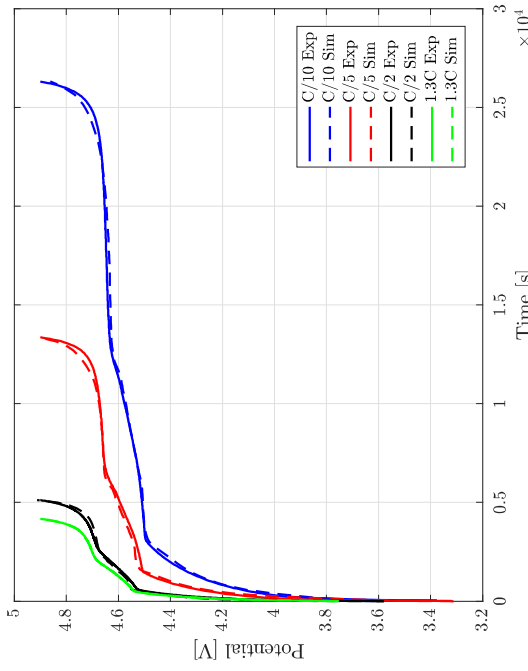


**Figure 6.** Comparison between the experimental and simulated charge curves at different charge currents.

intercalation reaction in the positive electrode of  $3.996 \text{ A m}^{-2}$  and a value of the double layer capacitance equal to  $2.5 \cdot 10^{-2} \text{ F}$ . Thus, the exchange current density value is comparable to that previously reported in Ref. 39, in which an equivalent circuit model has been used (see Fig. 5a). Fig. 5b shows the comparison between the experimental and the simulated trends in Nyquist plots while Fig. 5c shows the Bode diagram comparison between the experimental and the simulated trends related to the electrochemical impedance analysis performed. As can be seen on Figs. 5b and 5c, the medium frequency part of the spectra representing a linear increase of impedance and related to lithium ions diffusion, the fitting seems to be more approximate. One explanation could be the choice of considering only surface Li ion diffusion in the model and not consider solid diffusion influence. In the higher frequency region, representing electrochemical reactions (including charge transfer and double layer reaction) the fitting is more precise.

**Electrochemical model validation.**—The second phase of validation was carried out taking as reference the charge curve at the second cycle of cells at 4 different charge/discharge currents, namely at C/2, C/5 and C/10. In such part of validation, it was necessary to modify only the initial state of charge of the electrodes. In literature, values of the anodic reaction rate constants ranging from  $8.19 \cdot 10^{-12} \text{ m}^{-1} \text{s}$  to  $5.10^{-11} \text{ m}^{-1} \text{s}$  are reported.<sup>34,40</sup> For simulations, the value of  $2.10^{-11} \text{ m}^{-1} \text{s}$  well fits the experimental curves. For the diffusive coefficient of the negative electrode, different values are found in literature ranging from  $2.10^{-14} \text{ m}^2 \text{ s}^{-1}$  to  $9.10^{-14} \text{ m}^2 \text{ s}^{-1}$ .<sup>28,34,41-45</sup>

**Table II.** Input electrodes parameters used for the simulations.

Quantity	Unit	Negative electrode	Positive electrode	Value
Particle radius	$\mu\text{m}$	9.93	4.5	$5 \cdot 10^{-6}$
Maximum concentration solid phase	$\text{mol m}^{-3}$	31370	24358	0.16
Double layer capacity	$\text{F m}^{-3}$	0.5	$2.5 \cdot 10^{-2}$	0.8
Exchange current density	$\text{A m}^{-2}$	-	3.996	$1 \cdot 10^{-3}$
Reaction rate constant	$\text{m}^{-1} \text{s}$	$2 \cdot 10^{-1}$	-	250
Electrical conductivity	$\text{S m}^{-1}$	$2.01 \cdot 10^{-1}$	$2.54 \cdot 10^{-2}$	7

**Table III.** Input aging parameters used for the simulations.

Quantity	Unit	Value
SEI layer conductivity	$\text{S m}^{-1}$	$5 \cdot 10^{-6}$
Molar mass of product of side reaction	$\text{kg mol}^{-1}$	0.16
Density of products of SEI reaction	$\text{kg m}^{-3}$	1600
Aging parameter $\alpha$	-	-
Aging parameter J	-	-
Aging parameter f	$\text{s}^{-1}$	-
Aging parameter H	-	-

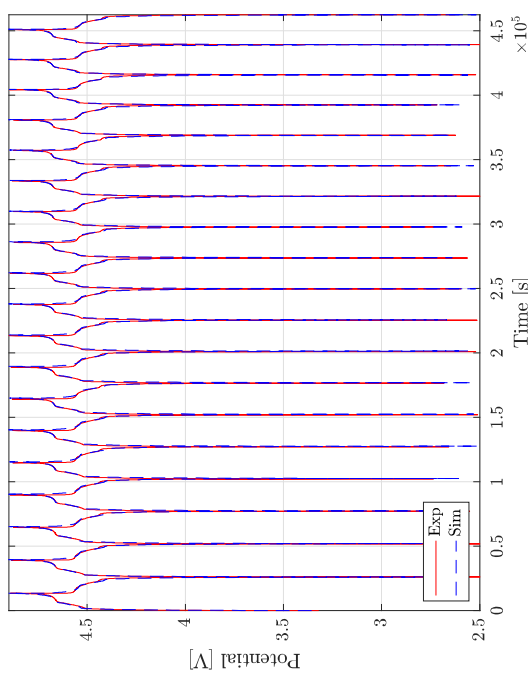


**Figure 7.** Comparison between the experimental and simulated trends of the potential as a function of time for the first 20 operating cycles of the cell at a current corresponding to C/5.

For simulations, the value of  $4.10^{-14} \text{ m}^2 \text{ s}^{-1}$  well fits charge and discharge curves. Fig. 6 shows the comparison between the experimental and simulated curves at different charge currents. The LNMO cathode shows two potential plateaus at 4.7 V and 4.0 V versus  $\text{Li}^+/\text{Li}$  which correspond to the  $\text{Ni}^{2+}/\text{Ni}^{3+}$  and  $\text{Mn}^{3+}/\text{Mn}^{4+}$  redox reactions, respectively.<sup>46</sup> The splitting of the model validation in these two phases allows the implementation of high accuracy model, thanks to the use of the results of the impedances as reference, since it allows to separate the behavior of the two electrodes and calibrate the cathode and anode parameters separately. It is possible to observe the model ability to precisely simulate the electrochemical behavior of the cell and the actual spectrum of the positive electrode.

**Aging model calibration.**—The aging model was validated using as reference the charge/discharge curves of the first twenty cycles of the cells at four different charge/discharge currents (C/5, C/2, C/5 and C/10) by using the aging parameters in Equation 26 as calibration parameters. To consider the Coulombic efficiency of the model, a different concentration of the active material for the charge and discharge phases was considered. The results obtained at C/5 are showed in Fig. 7, which reports the trend of the cell potential as a function of time during all cell cycles.

In Fig. 8a, the trends of the charge capacity are shown with respect to the number of cycles for C-rates equal to 1 and 0.5, respectively. Similar results were obtained for all the analyzed C-rate values.

Fig. 8b reports the trend of  $c_{SEI}$  with respect to the number of cell cycles. Table II shows all the parameters used in the simulation while Table III shows all the parameters related to the capacity fade model.

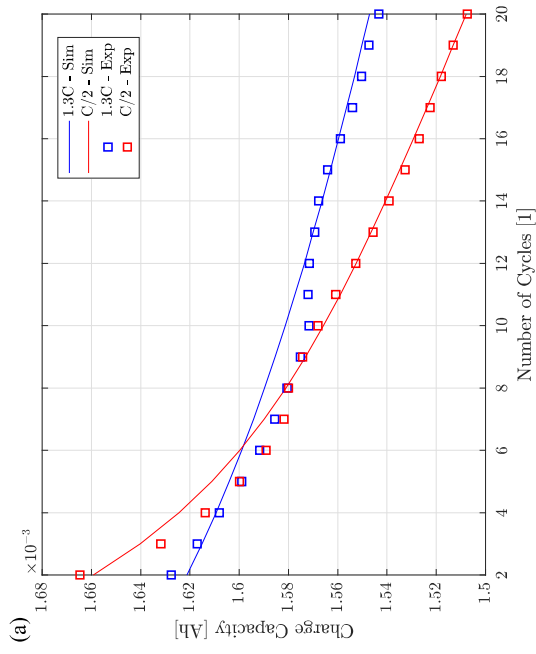


**Figure 8.** Experimental and simulated trends of the capacity (a) and of the simulated concentration of decomposition products from SEI reactions (b) as a function of the number of charge and discharge cycles performed by the cell.

As can be seen, the simulation results exhibit a very good match with the experimental data for this cycling scheme, perfectly predicting cell behavior.



**Figure 8.** Experimental and simulated concentration of decomposition products from SEI reactions (b) as a function of the number of cycles [1].

### Conclusions

A simple electrochemical model coupled with an aging model was successfully developed, combined with the electrochemical characterization of cell materials and validated. In particular, high voltage LNMO positive electrode was considered for the first time. The experimental analysis of the influence of the charge/discharge processes on SEI formation enlightened that lower currents favor SEI formation and therefore capacity fading. The implemented model represents the electrochemical behavior of the cell and its capacity fading due to SEI formation over the whole operating current range (C, C/2, C/5 and C/10) with optimal predictive capability. An inverse parameter determination of some of the model parameters has been discussed using numerical and analytical methods. The innovative approach used in this work consists in the iterative validation processes of the electrochemical model using the results of two different tests as references. In particular, the use of Electrochemical Impedance Spectroscopy as a reference to validate/calibrate the electrochemical model is fully innovative. This approach, as demonstrated in the present work is still at preliminary phases, giving therefore incomplete data for a thorough model validation. Future work will consist in comparison of experimental and modeling EIS for multiple conditions (e.g., state of charge) in order to validate the model robustness and flexibility toward predicting behavior at multiple conditions. As far as our knowledge is concerned, the high potential LNMO-based cathode used here is relatively new for modeling approaches. The present model provides the basis to better design and optimize high-potential cells for specific applications and thanks to the modular nature of the modeling approach, it can also be scaled up to battery models and packs.

### Acknowledgment

Authors kindly acknowledge Lithops S.r.l. for providing anodes and cathodes, ARKEMA for providing electrolytes and the E-Caiman project (G.A. 6533331, H2020 E.U.3.4.) for financial support.

### List of Symbols

Symbol	Description
$a_v$	Specific surface area
$c$	Volumetric concentration
CMC	Carboxymethyl cellulose
$D$	Diffusivity
$\epsilon$	Volume fraction
$F$	Faraday constant
$f$	Frequency
$I$	Current
$i$	Current density
$i_0$	Exchange current density
$k$	Rate constant
$L_{sep}$	Total thickness of separators
$L_i\theta_s$	Occupied reaction site on the surface of the electrodes active materials
LIBs	Lithium-ion batteries
OCV	Open Circuit Voltage
P2D	Pseudo two-dimensional model
PM	Molecular weight
$P_{SEI}$	Products of the electrolyte degradation reactions
PvDF	Polyvinylidene fluoride
$r$	Radius dimension
SBR	Styrene-butadiene
SEI	Solid Electrolyte Interphase
SoC	State of Charge
$S$	Electrolyte solvent
$V$	Voltage

### Greek

$\eta$	Over potential
$\rho_{el}$	Electrical resistivity
$\sigma$	Electrical conductivity
$\tau$	Tortuosity
$\theta_s$	Free reaction site on the surface of the electrodes active materials

### ORCID

Silvia Bodardo  <https://orcid.org/0000-0002-3579-9778>

## References

- J. M. Tarascon and M. Armand, "Issues and challenges facing rechargeable lithium batteries," *Materials for Sustainable Energy*, 171 (2010).
- J. M. Tarascon and M. Armand, "Building better batteries," *Nature*, **451**, 652 (2008).
- N. Nitta, F. Wu, J. T. Lee, and G. Yushin, "Li-ion battery materials: present and future," *Materials Today*, **18**(5), 252 (2015).
- M. Doyle, "Modeling of galvanostatic charge and discharge of the lithium/polymerinsertion cell," *Journal of The Electrochemical Society*, **140**(6), 1526 (1993).
- A. A. Franco, A. Rucci, D. Brandell, C. Frayret, M. Gaberscek, P. Jankowski, and P. Johansson, "Boosting Rechargeable Batteries R&D by Multiscale Modeling: Myth or Reality?" *Chemical Reviews*, **119**(7), 4569 (2019).
- C. Delacourt and M. Saffari, *Mathematical modeling of Li-Ion batteries, Physical Multiscale Modeling and Numerical Simulation of Electrochemical Devices for Energy Conversion and Storage* 151 (2016). Springer, London.
- A. Jokar, B. Rajabloo, M. Désilets, and M. Larroche, "Review of simplified Pseudo-two-Dimensional models of lithium-ion batteries," *Journal of Power Sources*, **327**, 44 (2016).
- A. Maheshwari, M. A. Dumitrescu, M. Destro, and M. Santarelli, "Inverse parameter determination in the development of an optimized lithium iron phosphate - graphite battery discharge model," *Journal of Power Sources*, **307**, 160 (2016).
- J. Newman and W. Tiedemann, "Porous electrode theory with battery applications," *AIChE Journal*, **21**(1), 25 (1975).
- T. F. Fuller, "Simulation and optimization of the dual lithium ion insertion cell," *Journal of The Electrochemical Society*, **132**(1), 5 (1985).
- D. Bernardi, "A general energy balance for battery systems," *Journal of The Electrochemical Society*, **121**(10), 25 (1974).
- T. F. Yi, J. Mei, and Y. R. Zhu, "Key strategies for enhancing the cycling stability and rate capacity of LiNi<sub>0.5</sub>Mn<sub>1.5</sub>O<sub>4</sub> as high-voltage cathode materials for high power Lithium-ion batteries," *Journal of Power Sources*, **316**, 85 (2016).
- Y. Dong, J. Demeneux, Y. Zhang, M. Xu, L. Zhou, A. D. MacIntosh, and B.-L. Lucht, "Improving the performance at elevated temperature of high voltage graphite/LiNi<sub>0.5</sub>Mn<sub>1.5</sub>O<sub>4</sub> cells with added lithium catenol dimethyl borate," *Journal of The Electrochemical Society*, **164**(1), 1 (1994).
- P. F. Yi, J. Mei, and Y. R. Zhu, "Key strategies for enhancing the cycling stability and rate capacity of LiNi<sub>0.5</sub>Mn<sub>1.5</sub>O<sub>4</sub> as high-voltage cathode materials for high power Lithium-ion batteries," *Journal of Power Sources*, **316**, 85 (2016).
- C. Arbizhani, F. D. Giorgio, L. Porcarelli, M. Mastragostino, V. Khomenko, V. Barsukov, D. Bresser, and S. Passerini, "Use of non-conventional electrolyte salt and additives in high-voltage graphite/ LiNi<sub>0.4</sub>Mn<sub>1.6</sub>O<sub>4</sub> batteries," *Journal of Power Sources*, **258**, 17 (2013).
- S. Monaco, F. D. Giorgio, L. D. Col, M. Riché, C. Arbizhani, and M. Mastragostino, "Electrochemical performance of LiNi<sub>0.5</sub>Mn<sub>1.5</sub>O<sub>4</sub> composite electrodes featuring carbon and reduced graphene oxide," *Journal of Power Sources*, **278**, 733 (2015).
- M. Mancini, P. Axmann, G. Gabrielli, M. Kintyajui, U. Kaiser, and M. Wohlfahrt-Mehrens, "A high-voltage and high-capacity Li<sub>1-x</sub>Ni<sub>0.3</sub>Mn<sub>1.5</sub>O<sub>4</sub> cathode material: From synthesis to full lithium-ion cells," *ChemSusChem*, **9**(14), 1843 (2016).
- P. Axmann, G. Gabrielli, and M. Wohlfahrt-Mehrens, "Tailoring high-voltage and high-performance LiNi<sub>0.5</sub>Mn<sub>1.5</sub>O<sub>4</sub> cathode material for high energy lithium-ion batteries," *Journal of Power Sources*, **301**, 151 (2016).
- J.-H. Kim, C. S. Yoon, S.-T. Myung, J. Prakash, and Y.-K. Sun, "Phase transitions in Li<sub>1-x</sub>Ni<sub>0.5</sub>Mn<sub>1.5</sub>O<sub>4</sub> during cycling at 5 V," *Electrochemical and Solid-State Letters*, **7**(7), A216 (2004).
- L. Wang, H. Li, X. Huang, and E. Baudrin, "A comparative study of  $\text{fd}\text{-}3\text{m}$  and  $\text{p}\text{-}3\text{3}2$  " $\text{LiNi}_{0.5}\text{Mn}_{1.5}\text{O}_4$ ," *Solid State Ionics*, **193**(1), 32 (2011).
- L. Valdes, "Resistivity measurements on germanium for transistors," *Proceedings of the IRE*, **42**(2), 20 (1954).
- M. Guo and R. E. White, "A distributed thermal model for a Li-ion electrode plate pair," *Journal of Power Sources*, **221**, 334 (2013).
- L. Saw, Y. Ye, and A. Tay, "Electrochemical-thermal analysis of 18650 lithium iron phosphate cell," *Energy Conversion and Management*, **75**, 162 (2013).
- A. Nyman, M. Behm, and G. Lindbergh, "Electrochemical characterization and modelling of the mass transport phenomena in LiPF<sub>6</sub>-EC-EMC electrolyte," *Electrochimica Acta*, **53**(22), 6356 (2008).
- C. Delacourt and M. Saffari, "Life simulation of a graphite/LiFePO<sub>4</sub> cell under cycling and storage," *Journal of The Electrochemical Society*, **159**(8), A1283 (2012).
- H. J. Plohn, P. Ramadas, and R. E. White, "Solvent diffusion model for aging of lithium-ion battery cells," *Journal of The Electrochemical Society*, **151**(3), A456 (2004).
- A. J. Smith, J. C. Burns, X. Zhao, D. Xiong, and J. R. Dahn, "A high precision coulometric study of the SEI growth in Li/graphite cells," *Journal of The Electrochemical Society*, **158**(5), A447 (2011).
- P. Ramadas, B. Haran, P. M. Gonadam, R. White, and B. N. Popov, "Development of first principles capacity fade model for Li-ion cells," *Journal of The Electrochemical Society*, **151**(2), A196 (2004).
- G. Ning, R. E. White, and B. N. Popov, "A generalized cycle life model of rechargeable Li-ion batteries," *Electrochimica Acta*, **51**(10), 2012 (2006).
- H. Ekstrom and G. Lindbergh, "A model for predicting capacity fade due to SEI formation in a commercial graphite/LiFePO<sub>4</sub> cell," *Journal of The Electrochemical Society*, **162**(6), A1003 (2015).
- A. Uhlig, "The Potentials of Infinite Systems of Sources and Numerical Solutions of Problems in Semiconductor Engineering," B.S.T.J., **105** (1955)
- F. M. Smits, "Measurement of sheet resistivities with the four-point probe," *Bell System Technical Journal*, **37**(3), 711 (1958).
- U. S. Kasarajuula, C. Wang, and P. E. Arec, "Discharge model for LiFePO<sub>4</sub> accounting for the solid solution range," *Journal of The Electrochemical Society*, **155**(1), A866 (2008).
- M. Saffari and C. Delacourt, "Modeling of a commercial graphite/LiFePO<sub>4</sub> cell," *Journal of The Electrochemical Society*, **158**(5), A562 (2011).
- V. Srinivasan and J. Newman, "Discharge model for the lithium iron-phosphate electrode," *Journal of The Electrochemical Society*, **151**(10), A1517 (2004).
- V. Thorat, T. Joshi, K. Zaghbi, J. N. Hanb, and D. R. Wheeler, "Understanding rate-limiting mechanisms for Li-ion batteries," *Journal of The Electrochemical Society*, **158**(11), A1185 (2011).
- D. A. Stevens and J. R. Dahn, "The mechanisms of lithium and sodium insertion in carbon materials," *Journal of The Electrochemical Society*, **148**(8), A803 (2001).
- D. P. Di Vincenzo, C. D. Fuerst, and J. E. Fischer, "(p,t) phase boundary in Li-intercalated graphite: Theory and experiment," *Physical Review B*, **29**(2), 1115 (1984).
- T. F. Yi, C. Y. Li, Y. R. Zhu, R. S. Zhu, and J. Shu, "Electrochemical intercalation kinetics of lithium ions for spinel LiNi<sub>0.5</sub>Mn<sub>1.5</sub>O<sub>4</sub> cathode material," *Russian Journal of Electrochemistry*, **46**(2), 227 (2010).
- K. Kumaresan, G. Sikha, and R. E. White, "Thermal model for a Li-ion cell," *Journal of The Electrochemical Society*, **155**(2), A164 (2008).
- N. Takami, "Structural and kinetic characterization of lithium intercalation into carbon anodes for secondary lithium batteries," *Journal of The Electrochemical Society*, **142**(2), 371 (1995).
- M. W. Verbrugge and B. J. Koch, "Electrochemical analysis of lithiated graphite anodes," *Journal of The Electrochemical Society*, **150**(3), A374 (2003).
- V. Srinivasan and J. Newman, "Design and optimization of a natural graphite/iron phosphate lithium-ion cell," *Journal of The Electrochemical Society*, **151**(10), A1530 (2004).
- M. Doyle and Y. Fuentes, "Computer simulations of a lithium-ion polymer battery and implications for higher capacity next-generation battery designs," *Journal of The Electrochemical Society*, **150**(6), A706 (2003).
- E. Prada, D. D. Domenech, Y. Creff, J. Bernard, V. Sauvant-Meynet, and F. Huet, "Simplified electrochemical and thermal model of LiFePO<sub>4</sub>-graphite Li-ion batteries for fast charge applications," *Journal of The Electrochemical Society*, **159**(9), A1508 (2012).
- C. M. Julian and A. Mauger, "Review of 5-V electrodes for Li-ion batteries: status and trends," *Ionics*, **19**(7), 951 (2013).